

Temporal clustering of rotational glitches in the Crab pulsar

J. B. Carlin,¹ A. Melatos,^{1,2} and D. Vukcevic^{3,4}

¹*School of Physics, University of Melbourne, Parkville, VIC 3010, Australia*

²*Australian Research Council Centre of Excellence for Gravitational Wave Discovery (OzGrav)*

³*School of Mathematics and Statistics, University of Melbourne, Parkville, VIC 3010, Australia*

⁴*Melbourne Integrative Genomics, University of Melbourne, Parkville, VIC 3010, Australia*

Accepted XXX. Received YYY; in original form ZZZ

ABSTRACT

It is an open question whether glitch activity in individual pulsars varies on decadal time-scales. The Crab pulsar has experienced 23 spin-up glitches in the last 36 years, interrupting an otherwise monotonic deceleration. A homogeneous Poisson process, i.e. a process with constant rate, is not sufficient to describe the time-ordered distribution of glitch epochs in the Crab pulsar. There are signs of clustering at the 2σ level when testing with Ripley’s K function. Two alternative, inhomogeneous models with one and two step-wise rate changes are found to have higher relative evidence (Bayes factors of 1.74 and 2.86 respectively) than the homogeneous Poisson process. The distinction between clustering, where events are correlated, and rate variation is discussed. The implications for glitch microphysics, in particular trigger mechanisms based on avalanche processes, are briefly discussed.

Key words: pulsars: general – stars: neutron – methods: statistical

1 INTRODUCTION

Rotation-powered pulsars spin down monotonically as they age due to electromagnetic braking (Taylor et al. 1993). The secular spin down is perturbed by continuous, stochastic “timing noise” (Cordes & Helfand 1980; Arzoumanian et al. 1994; Hobbs et al. 2010) as well as impulsive spin-up events called “glitches” (Melatos et al. 2008; Espinoza et al. 2011; Fuentes et al. 2017). Glitch rates and sizes appear to be uncorrelated in most pulsars (Melatos et al. 2018), with PSR J0537–6910 being a notable exception (Middleditch et al. 2006; Ferdman et al. 2017). However the datasets are small: 531 (386) glitches have been observed in total from 187 (132) pulsars¹ (Espinoza et al. 2011; Yu et al. 2013). Several glitch trigger mechanisms have been proposed including starquakes (Larson & Link 2002; Negi 2007), superfluid vortex avalanches (Anderson & Itoh 1975; Cheng et al. 1988; Warszawski & Melatos 2011; Warszawski et al. 2012), and magnetospheric phase transitions (Keith et al. 2013) among others; see Haskell & Melatos (2015) for a modern review.

A systematic study of the clustering of glitch epochs has not been undertaken across the known population of glitching pulsars, because until recently the samples per pulsar were too small to reliably infer clustering or rate changes. Gradually, however, the situation is improving. It is now possible to disaggregate the data and construct statistically reliable size and waiting time probability density functions for several objects (Melatos et al. 2008; Howitt et al. 2018) and study their size–waiting-time correlations (Fulgenzi et al. 2017; Melatos et al. 2018). Temporal clustering may offer a way to distinguish glitch models based on vortex avalanches and starquakes. The study of clustering of terrestrial earthquakes is a large and evolving field. For example, Omori’s Law phenomenologically describes the observed behaviour of aftershocks following a large earthquake (Omori 1894; Utsu et al. 1995). Likewise, with the advent of Gross-Pitaevskii simulations, it is possible to calculate clustering in superfluid vortex avalanches theoretically (Warszawski & Melatos 2011; Warszawski et al. 2012; Warszawski & Melatos 2013; Fulgenzi et al. 2017). Neutron star glitches exhibit signs of self-organised criticality (SOC) (Melatos et al. 2008). Whether all SOC systems show signs of temporal clustering is not yet clear (Kagan & Jackson 1991; Jensen 1998; Turcotte 1999; Kagan 2011; Aschwanden et al. 2018).

An analysis of the Crab pulsar’s glitch epochs was carried out by Lyne et al. (2015), who claimed that “the glitches are more clustered than can be expected from a random oc-

¹ Catalogues of pulsar glitches are maintained independently by the Jodrell Bank Centre for Astrophysics at <http://www.jb.man.ac.uk/pulsar/glitches.html> and the Australia Telescope National Facility (ATNF) at <http://www.atnf.csiro.au/research/pulsar/psrcat/glitchTbl.html>. Numbers in the text without (with) parentheses refer to Jodrell Bank (ATNF) data and are current as of 2018 September 12.

currence of glitches” (verbatim quote). In this paper, we re-analyse the latter data in order to test the hypothesis, that the Crab’s glitches can be modelled as a homogeneous (i.e. constant rate) Poisson process. We review the observations in Section 2. In Section 3 we test for clustering in the Crab’s glitches using Ripley’s K function (Ripley 1977, 1988), under the null hypothesis of a homogeneous rate. We emphasize that clustering and rate changes are different things, as explained in Section 3. We then model the Crab’s glitch activity as a Poisson process that changes rate exactly once in Section 4. In Section 5 we model the Crab’s glitch activity as a Poisson process with two discrete rate changes. We do a pairwise Bayesian comparison between the one-, two-, and three-rate models in Section 6.

2 OBSERVATIONS

Daily observations of the Crab pulsar have been carried out by the Jodrell Bank Observatory since 1982, mainly using the 13m radio telescope at 610 MHz (Lyne et al. 1988, 1993). These observations are supplemented by earlier, less regular data from the Arecibo Observatory (Gullahorn et al. 1977), and with observations in the optical from the Princeton University Observatory (Groth 1975) and Hamburg Observatory (Lohsen 1981). An overview of the last 45 years of Crab pulsar observation can be found in Lyne et al. (2015).

Although 27 glitches have been directly observed, the analysis in Lyne et al. (2015) is restricted to the 20 glitches that occurred between Modified Julian Date (MJD) 45028 and MJD 55876, as that is when high-cadence monitoring occurred at the Jodrell Bank Observatory. The cut aims to remove the effect that the 3-yr gap in monitoring (between 1979 and 1982) may have on the completeness of the dataset. In this paper we analyse the 23 glitches between MJD 45028 and MJD 58380, as three more glitches have occurred since 2015, on MJD 57840, MJD 58065, and MJD 58237 (Shaw et al. 2018). The data from the last 36 years constitutes a statistically complete set, in the sense specified in section 3.2 of Espinoza et al. (2014).

2.1 Waiting times

For the 23 events between MJD 45028 and MJD 58380, the average waiting time between consecutive glitches is 526.08 days. The epochs, t_i , and fractional sizes ($\Delta\nu/\nu$, where $\Delta\nu$ is the glitch size, and ν is the spin frequency), can be seen in the top panel of Figure 1. Henceforth t_i corresponds to the epoch of the i -th glitch. The bottom panel plots the empirical cumulative distribution function (CDF) for the waiting times between consecutive glitches (blue curve) as well as a 2σ envelope of synthetic CDFs drawn from a Monte Carlo sampling of 10^5 homogeneous Poisson processes (black curve, mean; shaded grey region, 2σ spread), where 23 events occur in 36 years.² Waiting times are distributed exponentially in a homogeneous Poisson process. A Kolmogorov-Smirnov

² We model a homogeneous Poisson process conditional on observing exactly 23 events in 36 years by drawing 23 glitch epochs from a uniform distribution and taking the difference between consecutive epochs to find the waiting times between glitches. This is not equivalent to drawing 22 numbers from an exponen-

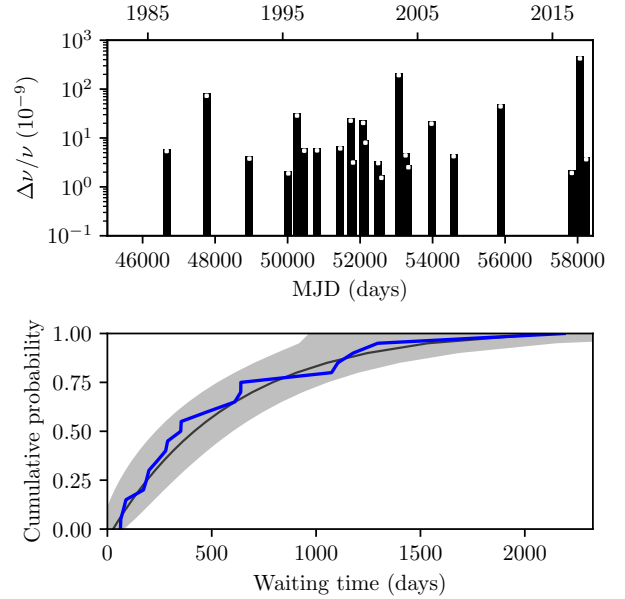


Figure 1. (Top panel.) Epochs and fractional sizes of the Crab’s 23 glitches observed from MJD 45028 (1982) to MJD 58380 (2018). (Bottom panel.) Empirical CDF of the 22 observed waiting times between consecutive events (blue curve) and for synthetic waiting times generated by a homogeneous Poisson process, conditional on 23 events occurring in 36 years (black curve, mean; shaded grey region 2σ spread; 10^5 realizations).

test (Lilliefors 1969) does not support rejecting the null hypothesis, that the 22 inter-glitch waiting times are drawn from an exponential distribution (p-value of 0.39).

2.2 Preliminary evidence of clustering

The Kolmogorov-Smirnov test above involves a summary statistic of the full, time-ordered dataset of glitch epochs. It only tests one property of the process, namely that waiting times between consecutive events are distributed exponentially. It should not be interpreted to imply that a homogeneous Poisson process is the best or only model for the data.

Lyne et al. (2015) extended this type of test by calculating the empirical CDF of the waiting times between all pairs of glitch epochs (see Section 3 of the latter reference). They concluded that a homogeneous Poisson process does not adequately model the Crab’s glitch activity. Figure 6 in Lyne et al. (2015) is reproduced in Figure 2 of this manuscript. It shows the CDF of 253 all-pair waiting times, $\Delta t'$. Clustering is indicated if the CDF is steeper at small $\Delta t'$ than the null model—that the glitch epochs are distributed as a homogeneous Poisson process—as this shows that there are more events grouped together than what is expected, if the glitch epochs obey the null model. Figure 2 shows that the Crab’s glitches appear to be clustered, as the Crab’s CDF is 2σ above the mean CDF constructed synthetically from a

tial distribution with mean equal to the observed average waiting time (Baddeley et al. 2015).

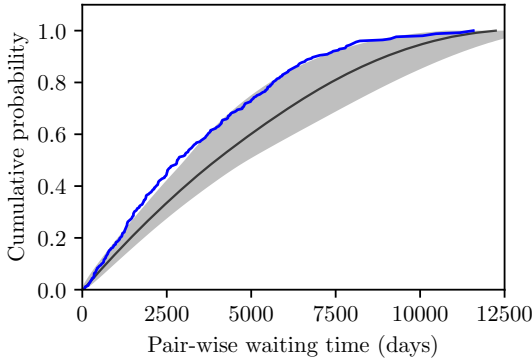


Figure 2. Cumulative distribution function of the 253 waiting times between all pairs of glitch epochs for the Crab (blue curve) and for a synthetic homogeneous Poisson process, where 23 events occur in 36 years (black curve, mean; shaded grey region, 2σ spread; 10^5 realizations). [Based on Figure 6 in Lyne et al. (2015).]

homogeneous Poisson process at the point of greatest difference. This test resembles Ripley’s K statistic (Ripley 1977, 1988) but does not include an edge correction term, as discussed in the following section.

3 CLUSTERING

Upon visual inspection, the 14 glitches between MJD 50000 and 53800, in the top panel in Figure 1, appear to be clustered more closely than the three glitches between MJD 45028 and MJD 50000, and the six glitches between MJD 53800 and MJD 58380. We now test rigorously whether there is statistically significant evidence of clustering.

3.1 Ripley’s K function

An extension of the test used by Lyne et al. (2015) is to use Ripley’s K function (Ripley 1977, 1988) to test for clustering at a level higher than what is expected for a homogeneous Poisson process. Ripley’s K function is used widely for this purpose in ecology (Kenkel 1988; Peterson & Squiers 1995), biology (Jafari-Mamaghani 2010; Lagache et al. 2013), geoscience (Vega Orozco et al. 2012), and physics (Loh 2008; White et al. 2012). Ripley’s K function was applied to one-dimensional spatial data by Yunta et al. (2014) but it also works for one-dimensional temporal data, such as glitch epochs.

Before we continue we emphasize that a process with clustering is not the same as a process with a variable rate. For example, in an inhomogeneous Poisson process, each event is independent, but the underlying rate varies. Often the underlying cause for the rate change is external and can be measured or estimated in another way. In contrast, in clustered processes (e.g. Cox or Gibbs), the occurrence of events is correlated, and the underlying rate need not vary. Often the cause of the clustering is endogenous (Baddeley et al. 2015). Distinguishing between clustering and an inhomogeneous Poisson process is not possible from looking at a sequence of events (Bartlett 1964; Gelfand et al. 2010); it

is always possible to find a time-varying rate that produces the same distribution of epochs as a cluster model.

Ripley’s K function calculates the over- or under-occurrence of clusters of events in an ordered sequence. It compares to a null hypothesis of what is expected from a homogeneous Poisson process. Precisely, Ripley’s K function counts the number of events that occur within a sliding window of length w ,

$$K(w, n) = \frac{T}{n(n-1)} \sum_{i \neq j} H(w - \Delta t_{ij}) e_{ij} , \quad (1)$$

with $\Delta t_{ij} = |t_i - t_j|$. In (1), n is the total number of events in $0 \leq w \leq T$. $H()$ is the Heaviside function. The sum counts how many pairs are composed of events that occur within w of each other, weighted by an edge correction factor e_{ij} . The edge correction we use here is a variant of Ripley’s correction (Ripley 1988) for one-dimensional data [see Yunta et al. (2014) for details]:

$$e_{ij} = \frac{1}{2} [g(t_i, t_j) + g(t_j, t_i)] , \quad (2)$$

with

$$g(t_i, t_j) = 1 + H[\Delta t_{ij} - \min(t_i, T - t_i)] . \quad (3)$$

That is, events that occur closer to each other in time than to either edge of the observation window are weighted more heavily. This accounts for the fact that edge events may have more neighbours outside the observation window, which are not observed.

The theoretical K function in one dimension, with the edge correction specified above, has the following mean and variance (Yunta et al. 2014):

$$\mathbb{E}[K(w, n)] = 2w , \quad (4)$$

and

$$\text{var}[K(w, n)] = \frac{4T}{n(n-1)} \left[w - \frac{5w^2}{4T} + \frac{(n-2)w^3}{6T^2} \right] . \quad (5)$$

Given (4) and (5) we can introduce a normalised statistic $\tilde{K}(w, n)$ with zero mean and unit variance,

$$\tilde{K}(w, n) = \frac{K(w, n) - \mathbb{E}[K(w, n)]}{\sqrt{\text{var}[K(w, n)]}} . \quad (6)$$

3.2 Application to the Crab pulsar’s glitches

The probability density function (PDF) of \tilde{K} is a normal distribution in the limit $n \gg 1$ (Lang & Marcon 2010; Yunta et al. 2014). For intermediate and small values of n , the probability density function is not known analytically. However quantiles can be calculated from Monte Carlo simulations. Hypothesis testing is performed by comparing the empirical \tilde{K} statistic for the Crab to the \tilde{K} statistic for the null hypothesis of a homogeneous Poisson process. The homogeneous Poisson process is the natural null for this statistic. Explicitly, we use a Monte Carlo method to generate 23 glitch epochs from the null homogeneous Poisson process model 10^5 times, find \tilde{K} for each simulation, and compare the spread of \tilde{K} with the empirical \tilde{K} statistic for the Crab’s 23 glitch epochs.

The results of the above test are shown in Figure 3. The empirical \tilde{K} statistic for the Crab exceeds the 2σ envelope

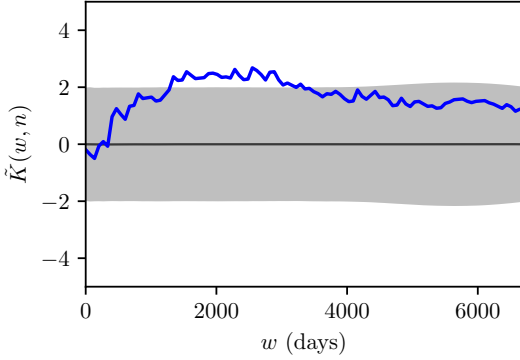


Figure 3. Empirical \hat{K} function for the Crab (blue curve), compared to a synthetic, homogeneous Poisson process, where 23 events occur in 36 years (black curve, mean; shaded grey region, 2σ spread; 10^5 realizations).

of the simulations for $1400 \text{ days} \lesssim w \lesssim 3000 \text{ days}$. Hence we can say that, under the assumption of a homogeneous Poisson process, the Crab’s glitches exhibit clustering above 2σ significance for time-scales $1400 \text{ days} \lesssim w \lesssim 3000 \text{ days}$. This is qualitatively concordant with the results of the test done by [Lyne et al. \(2015\)](#), where the empirical statistic for the Crab (in their case the CDF of waiting times between all pairs of glitches) sits outside the 2σ simulation envelope of the null homogeneous Poisson process, for all-pair waiting times between 1.4×10^3 and 8.0×10^3 days; see Figure 6 in [Lyne et al. \(2015\)](#) and Figure 2 in this manuscript.

4 POISSON PROCESS WITH ONE DISCRETE RATE CHANGE

An exponential waiting-time PDF, which is characteristic of a homogeneous (i.e. constant rate) Poisson process, is an adequate fit for the 22 waiting times in Figure 1. However there are many other ways to get an approximately exponential waiting-time PDF, for example a state-dependent Poisson process ([Fulgenzi et al. 2017](#)), which is inhomogeneous. The evidence of clustering found in Section 3 indicates that a homogeneous Poisson process is not sufficient to model the specific, time-ordered sequence of glitch epochs. It is therefore interesting to ask what simple inhomogeneous models could reasonably explain the data. We first explore a piecewise homogeneous Poisson process with a single, instantaneous rate change at the epoch T_1 . We propose this model because it is simple, inhomogeneous, and can be extended easily by adding additional rate jumps.

4.1 Joint probability density

To test for a single rate change, we note that the waiting times, Δt_i , between consecutive glitches are distributed exponentially for a Poisson process, i.e. the probability density function for the waiting time Δt_i is

$$f(\Delta t_i) = \lambda_i e^{-\lambda_i \Delta t_i} \quad (7)$$

where λ_i is the rate (assumed constant) in the interval between the two glitches, at epochs t_i and t_{i+1} . The complemen-

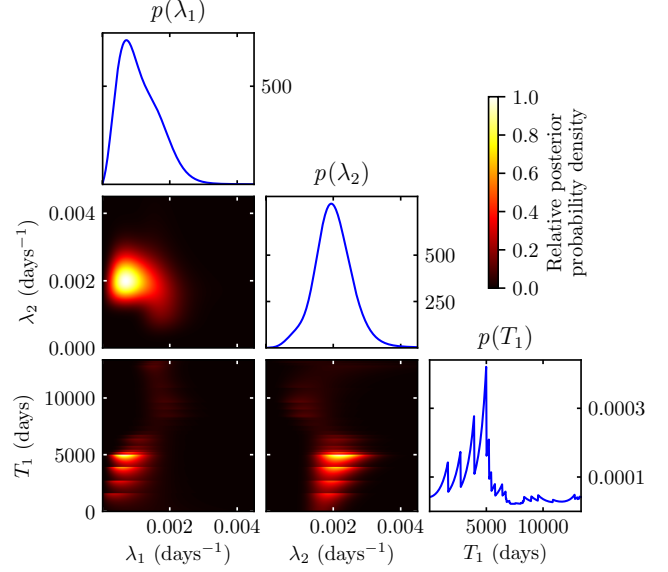


Figure 4. Posterior PDF, $\Pr(\lambda_1, \lambda_2, T_1 | D)$, for the piecewise homogeneous Poisson process with a single rate change at the epoch T_1 , marginalized over all combinations of parameters. The bottom-left panel is the posterior marginalized over λ_2 , the bottom-middle panel is the posterior marginalized over λ_1 , and the middle-left panel is the posterior marginalized over T_1 . Single-variable marginal posteriors are also plotted for λ_1 (top-left), λ_2 (middle), and T_1 (bottom-right). In the two-variable panels the maximum probability point is scaled arbitrarily to unity.

tary CDF, $F(\Delta t_i)$, which gives the probability of not seeing an event within an interval of length Δt_i , takes the form

$$F(\Delta t_i) = 1 - e^{-\lambda_i \Delta t_i} \quad (8)$$

Whenever the rate changes, there is a time period between two glitches that brackets the rate change, in which (7) does not apply. As the Poisson process is memoryless we can split up each interval between consecutive glitches into two sections, one of length τ_1 with rate λ_1 , the other of length τ_2 with rate λ_2 . The probability density of observing a waiting time of length Δt_i is the product,

$$f(\Delta t_i) = [1 - F(\tau_1)] f(\tau_2) \quad (9)$$

$$= \lambda_2 e^{-\lambda_1 \tau_1 - \lambda_2 \tau_2} \quad (10)$$

with $\Delta t_i = \tau_1 + \tau_2$. If the rate does not change within Δt_i (i.e. $\lambda_1 = \lambda_2$), we recover $f(\Delta t_i)$ in (7).

If we allow the rate to change once only, at the epoch T_1 , during the total observation of duration T , we can construct the joint probability of seeing the observed sequence of glitch epochs, $D = \{t_1, \dots, t_n\}$, where there are N_1 glitches before T_1 , and N_2 glitches after T_1 , by multiplying together the probability density for each consecutive waiting time Δt_i :

$$\Pr(D | \lambda_1, \lambda_2, T_1) = \prod_{i=1}^n f(\Delta t_i) \quad (11)$$

$$= \lambda_1^{N_1} e^{-\lambda_1 T_1} \lambda_2^{N_2} e^{-\lambda_2 (T - T_1)} \quad (12)$$

A discussion of an alternative, seemingly natural, yet

inappropriate likelihood function can be found in Appendix A.

4.2 Marginalized posteriors

The joint probability distribution (12) is a likelihood function, $L(\lambda_1, \lambda_2, T_1 | D)$, i.e. the probability of the data, D , given the parameter vector $(\lambda_1, \lambda_2, T_1)$. We assume a bounded uniform prior on T_1 , and gamma distribution priors for λ_1 and λ_2 to calculate the posterior probability density function, $\Pr(\lambda_1, \lambda_2, T_1 | D)$, for these parameters. The range allowed for T_1 covers the entire observation, i.e. $0 \leq T_1/(1 \text{ day}) \leq 1.34 \times 10^4$. The gamma distribution PDF

$$p(\lambda; k, \theta) = \frac{1}{\Gamma(k)\theta^k} \lambda^{k-1} e^{-\lambda/\theta}, \quad (13)$$

where $\Gamma(k)$ is the gamma function, has shape parameter $k = 2$ and scale parameter $\theta = (N_1 + N_2)/(kT) \approx 8.61 \times 10^{-4} \text{ days}^{-1}$, such that the mean equals the average rate observed over $0 \leq t \leq T$. The impact of the prior on the posterior and the Bayesian evidence is explored further in Section 6 and Appendix B. There are many valid ways to choose the prior, of course. Here we adopt the gamma distribution defined in (13), which is conjugate to the Poisson distribution in the sense described in Appendix B. Conjugate priors are commonly adopted in statistics in the absence of more specific prior knowledge. A bounded uniform prior for the rates is also defensible but it places a high probability for certain outcomes that are known to be a priori implausible by eyeballing the data, e.g. two simultaneously high rates. In contrast, the gamma distribution defined in (13) decreases to zero as λ increases, which is more realistic. Hence we prefer the gamma prior for the rates in this paper.

We can marginalise the full posterior probability, $\Pr(\lambda_1, \lambda_2, T_1 | D)$, over any one parameter to find the marginalized posterior probability of the other two. The results of marginalising can be seen in Figure 4. The two-dimensional heat maps (middle-left, bottom-left, and bottom-middle panels) show the joint likelihood of different pairs of parameters. The bottom-right panel indicates that a model with a rate change just before $T_1 \approx 5 \times 10^3$ days has the best support. This value of T_1 corresponds roughly to MJD 50000. In the middle-left panel, much of the probability mass lies off the diagonal, suggesting that there is little support for a homogeneous (constant rate) Poisson process. The marginalized posterior for T_1 is spiky, because (12) changes discontinuously when T_1 rolls over a glitch epoch, which increments N_1 and decrements N_2 . In contrast, the marginalized posteriors for λ_1 and λ_2 are smooth, because N_1 and N_2 are not functions of λ_1 and λ_2 .

5 POISSON PROCESS WITH TWO DISCRETE RATE CHANGES

We can also test whether the Crab's glitches can be modelled as a piecewise homogeneous Poisson process with two instantaneous rate changes, one at the epoch T_1 , the second at the epoch $T_2 > T_1$. This more elaborate model is inspired by the top panel of Figure 1, where there appear (to the eye) to be three distinct regimes of glitch activity: before the glitch at MJD 50000, between MJD 50000 and

MJD 53800, and after MJD 53800. We test for the two-rate-change model by extending (12) to the joint probability of observing the sequence of glitch epochs, D , where there are N_1 glitches in $0 \leq t < T_1$, N_2 glitches in $T_1 \leq t < T_2$, and N_3 glitches in $T_2 \leq t \leq T$, with constant rates λ_1 , λ_2 , and λ_3 respectively. The result is

$$\Pr(D | \lambda_1, \lambda_2, \lambda_3, T_1, T_2) = \lambda_1^{N_1} e^{-\lambda_1 T_1} \lambda_2^{N_2} e^{-\lambda_2 (T_2 - T_1)} \times \lambda_3^{N_3} e^{-\lambda_3 (T - T_2)}. \quad (14)$$

The joint probability defined by (14) is a likelihood function, as in Section 4, i.e. the probability of the data, D , given the parameter vector $(\lambda_1, \lambda_2, \lambda_3, T_1, T_2)$. We assume the same gamma distribution prior defined in Section 4 on all three rate parameters λ_1 , λ_2 , and λ_3 . For T_1 and T_2 we assume a uniform prior on the space of all possible values, which is the triangle (two-dimensional simplex) defined by the natural bounds on T_1 and T_2 , including $T_1 < T_2$. This triangle is depicted as the non-grey portion of the T_1 - T_2 panel in Figure 5.

The marginalised posterior PDF is shown in Figure 5. The panels along the diagonal from the top-left to the bottom-right show the one-dimensional marginalised posteriors for λ_1 , λ_2 , λ_3 , T_1 , and T_2 respectively. The sharp peak in $p(T_1)$ at $T_1 \approx 5 \times 10^3$ days corresponds to roughly MJD 50000. The three sharp peaks in $p(T_2)$ between 8×10^3 days and 10^4 days correspond to the three glitches following MJD 53800. In other words, when using two rate-change model, the data most supports one rate change occurring at around MJD 50000 and a second rate change occurring somewhere between MJD 53800 and MJD 54000. Broadly speaking, as the marginalised posteriors for T_1 and T_2 are approximately unimodal there is qualitative support for two rate changes fitting the Crab's glitches. However, this statement is purely qualitative. We assess its worth quantitatively in Section 6, through a formal model comparison using Bayes factors.

Another way to represent the posterior distribution is to pick an observation time, t^* , and construct a PDF for the value of the rate at that time, $\lambda(t^*)$. As this rate function is a piecewise constant function of the parameters in the model, the posterior distribution of $\lambda(t^*)$ is an integral of the full posterior distribution on the five parameters, $(\lambda_1, \lambda_2, \lambda_3, T_1, T_2)$. $\lambda(t^*)$ is a function of the posterior PDF, and as such uses all of the data, before and after t^* . We use a grid-based numerical integration method. The result is shown in Figure 6. This figure divides into roughly three regimes. $t^* \leq 5 \times 10^3$ days, where $\lambda(t^*) \approx 0.001 \text{ days}^{-1}$; $5 < t^*/(10^3 \text{ days}) \leq 8$, where $\lambda(t^*) \approx 0.0025 \text{ days}^{-1}$; and $t^* > 8 \times 10^3$ days, where $\lambda(t^*) \approx 0.0015 \text{ days}^{-1}$. We emphasise that the presence of three regimes is not surprising, because we are fitting a two-rate-change model. Nevertheless, this summary statistic derived from full posterior offers a way to visualize the uncertainty in the estimate of the rate function, given the choice of a two-rate-change model. The relative Bayesian evidence in the data for this model is calculated in Section 6.

6 BAYESIAN MODEL SELECTION

To quantitatively compare the relative goodness-of-fit for the homogeneous Poisson process (model M_0), one rate change

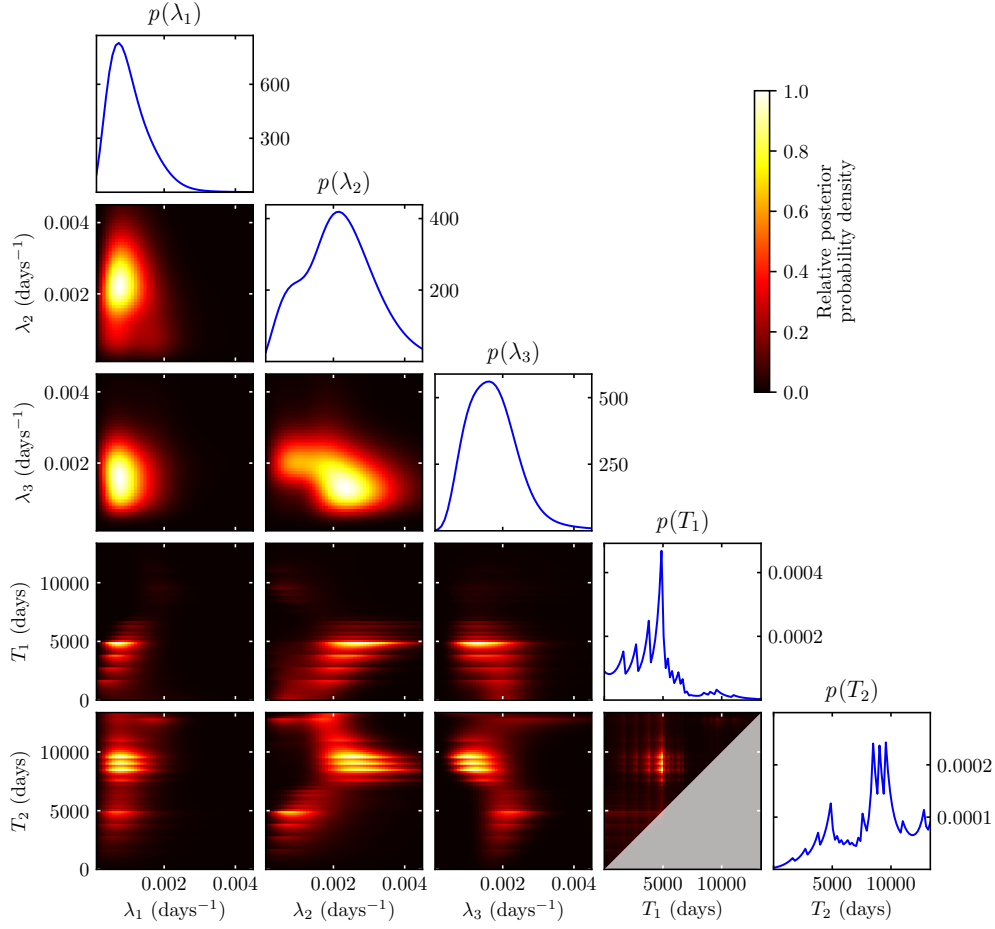


Figure 5. Posterior PDF, $\Pr(\lambda_1, \lambda_2, \lambda_3, T_1, T_2 \mid D)$, for the piecewise homogeneous Poisson process with two rate changes, one at the epoch T_1 , the other at the epoch T_2 , marginalized over all combinations of parameters. In the two-variable panels the maximum probability point is scaled arbitrarily to unity.

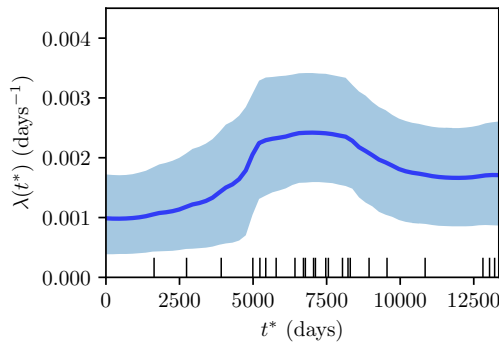


Figure 6. The solid blue curve shows the mean of the PDF $p[\lambda(t^*)]$ of $\lambda(t^*)$. The light blue band indicates the 10th and 90th percentile of each PDF. The small black ticks indicate the epochs of the 23 observed glitches.

Poisson process (M_1), and two rate change Poisson process (M_2), we compute the Bayesian evidence for M_0 , M_1 and M_2 by integrating the likelihood function over all parameters,

viz.

$$\text{Evidence}(M_i \mid D) = \int d\vec{\theta}_i L(M_i, \vec{\theta}_i \mid D) \Pr(\vec{\theta}_i) , \quad (15)$$

where $\Pr(\vec{\theta}_i)$ are the priors for the parameter vectors $\vec{\theta}_i$. Explicitly, the priors chosen for all models M_i are

$$\Pr(\lambda_1) = \text{Gamma}(\lambda_1; k = 2, \theta = 8.61 \times 10^{-4} \text{ days}^{-1}) , \quad (16)$$

and $\Pr(\lambda_1) = \Pr(\lambda_2) = \Pr(\lambda_3)$. For M_1 , we also have

$$\Pr(T_1) = U_1 (0 \text{ days} \leq T_1 \leq 1.34 \times 10^4 \text{ days}) . \quad (17)$$

For M_2 , we also have

$$\Pr(T_1, T_2) = U_2 (0 \text{ days} \leq T_1 < T_2 \leq 1.34 \times 10^4 \text{ days}) , \quad (18)$$

where U_1 and U_2 are normalized to unity. $\text{Gamma}(\lambda; k, \theta)$ refers to the gamma distribution defined in (13).

The integrals in (15) are performed using adaptive quadrature (Piessens et al. 1983). The results can be seen in Table 1. The absolute scale is not important for model selection. To compute the Bayes factor we take the ratio of the evidence for any two models. The ratio provides a scale on which to judge the relative evidence in the data

Model	Evidence ($\times 10^{-75}$)
M_0	7.56
M_1	13.14
M_2	21.62

Table 1. Bayesian evidence for the homogeneous Poisson process (model M_0), one rate change Poisson process (M_1), and two rate change Poisson process (M_2).

for two competing models. The largest Bayes factor is for M_2 over M_0 (Bayes factor 2.86). This is interpreted as “positive” or “substantial” evidence, depending on which standard scale one prefers (Kass & Raftery 1995; Jeffreys 1998). Bayesian evidence and Bayes factors automatically control for over-fitting (i.e. too many model parameters) by explicitly recognising and integrating over the prior distributions. If the likelihood of the data given two different models is the same, but one model has a larger prior parameter space, then it will have lower relative evidence compared to the other model (McElreath 2016). Broadly speaking, both inhomogeneous rate models M_1 and M_2 are favored over the null hypothesis of a homogeneous Poisson process (M_0), given the priors specified above. The sensitivity of the evidence to the parameters in the gamma distribution prior is explored in Appendix B.

7 CONCLUSIONS

Visual inspection of the epochs for the 23 Crab pulsar glitches between 1982 and 2018 suggests that they may be clustered and/or occur at a variable rate, with the 14 glitches between MJD 50000 and MJD 53800 seeming to occur more frequently than the rest. This visual observation was tested quantitatively by Lyne et al. (2015), who showed that the CDF for the waiting times between all glitch pairs cannot be modelled adequately as a homogeneous Poisson process. In this paper we look at the question from two perspectives, which complement the approach in Lyne et al. (2015). Specifically, (i) we test for clustering using Ripley’s K function, and (ii) we test the support for two alternative, inhomogeneous Poisson processes.

If we assume a homogeneous Poisson process, there are signs of clustering at 2σ significance for time-scales 1400 days $\lesssim w \lesssim$ 3000 days, as indicated by Ripley’s K function (Section 3). Assuming gamma distribution priors for the rates, inhomogeneous Poisson processes tested with one and two discrete rate changes are both favoured over a homogeneous Poisson processes, with Bayes factors of 1.73 and 2.86 respectively (Sections 4–6).

Although the glitch trigger mechanism is unknown, many discussions of the issue focus on avalanche processes, involving superfluid vortex motion or starquakes for example. In an avalanche process one must distinguish between two rates: (i) the rate at which the system is driven, which is set externally and is usually slow and constant; and (ii) the event rate, which is determined internally by the avalanche dynamics and fluctuates around a mean value. Therefore sequences of events observed during a short block of time (short compared to the time-scale of the external driver) can be interpreted in terms of rate changes or clustering; see Figure 24 in Fulgenzi et al. (2017). This result equally applies to

starquakes and superfluid vortex avalanches if the underlying processes involve a large number of interacting elements (e.g. tectonic plates, vortices) engaged in correlated, “knock-on” motion (Haskell & Melatos 2015), e.g. as in SOC systems (Jensen 1998). Processes that do not involve avalanches can also exhibit rate changes, e.g. temperature changes or a build up of differential rotation, but it is unclear why these would change markedly on decadal time-scales, and do so non-monotonically; see Figure 6.

Future work along these lines includes: (i) testing whether the data are Markovian, i.e. that a glitch waiting time depends solely on the previous waiting time (Cox & Lewis 1966; Çinlar 1975); (ii) treating the data as a marked Poisson process by introducing the additional information of glitch sizes (Kingman 1993); or (iii) applying the physically motivated state-dependent Poisson process proposed by Fulgenzi et al. (2017). Model fitting of any kind is greatly assisted by using all of the information available in the time-ordered sequence of events observed.

8 ACKNOWLEDGEMENTS

Parts of this research were conducted by the Australian Research Council Centre of Excellence for Gravitational Wave Discovery (OzGrav) through project number CE170100004. The authors would like to thank John Bowman at Walmart Labs (user “jbowman” on stats.stackexchange.com) for suggesting useful modifications to the likelihood function.

APPENDIX A: ALTERNATIVE JOINT PROBABILITY DISTRIBUTION

Instead of equation (12) one may be tempted to construct a different likelihood function of the form

$$\Pr(N_1, N_2 \mid \lambda_1, \lambda_2, T_1) = \frac{(\lambda_1 T_1)^{N_1} e^{-\lambda_1 T_1}}{N_1!} \times \frac{(\lambda_2 (T - T_1))^{N_2} e^{-\lambda_2 (T - T_1)}}{N_2!}, \quad (\text{A1})$$

because this is the joint probability of one Poisson distribution with N_1 events in a region of length T_1 , at a constant rate λ_1 , multiplied by another Poisson distribution with N_2 events in a region of length $(T - T_1)$, at a constant rate λ_2 . However, (A1) throws away most of the information about the timing of the glitches. It effectively splits the entire time-ordered dataset into only two samples, the sets of events before and after T_1 , and summarises each sample with an unordered count of the events. It therefore cannot distinguish properly between small T_1 with high λ_1 , or large T_1 with low λ_1 ; both scenarios have the same probability in (A1). In contrast, equation (12) assigns different probabilities to these scenarios. Hence (A1) is not the appropriate likelihood function to use when asking questions about the timing of events, which we need to do when testing whether the data can be modelled as an inhomogeneous Poisson process with one or two discrete rate changes.

k	$k\theta/\bar{\lambda}$	M_1/M_0	M_2/M_0
1	0.5	1.75	2.05
1	1.0	1.70	2.54
1	2.0	1.27	1.75
2	0.5	1.74	2.01
2	1.0	1.74	2.86
2	2.0	1.09	1.55
4	0.5	1.53	1.62
4	1.0	1.64	2.61
4	2.0	0.82	1.00

Table B1. Bayes factors for the one rate change Poisson process over the homogeneous Poisson process (M_1/M_0), and the two rate change Poisson process over the homogeneous Poisson process (M_2/M_0), for nine parameter sets ($k, k\theta/\bar{\lambda}$) defining the gamma distribution rate prior.

APPENDIX B: SENSITIVITY OF BAYESIAN EVIDENCE TO THE PRIOR

The gamma distribution assumed as the prior for the rates has the functional form given in (13). The gamma distribution is chosen because it is flexible and conjugate to a Poisson distribution, i.e. the likelihood multiplied by the prior is of the same functional form as the prior itself (Gelman et al. 2013). This allows for integrals over the likelihood and prior to be computed efficiently. Prior observational knowledge about the rate of events for the Crab pulsar, assuming a homogeneous Poisson process, indicates that the mean of the prior distribution should be comparable to the mean rate for Crab, i.e. $\bar{\lambda} = 23/(58380 - 45028) \approx 1.72 \times 10^{-3} \text{ days}^{-1}$. The mean of (13) is $k\theta$, so as our default choice we set $\theta = \bar{\lambda}/k$ in Sections 4–6. To test the sensitivity of the Bayesian evidence to this choice we test two alternative values of the mean, namely $k\theta = 0.5\bar{\lambda}$ and $k\theta = 2\bar{\lambda}$. We also test the sensitivity to changes in k . The Bayes factors for a few representative choices of these parameters are shown in Table B1.

In all nine parameter sets, the model with two rate changes, M_2 , has the highest evidence. The Bayes factors do not vary wildly from set to set. Broadly speaking, the evidence in favor of the two rate change model is consistent, regardless of the exact specification of the prior. This gives some confidence that the model truly captures an essential feature of the data.

REFERENCES

Anderson P. W., Itoh N., 1975, *Nature*, 256, 25
 Arzoumanian Z., Nice D. J., Taylor J. H., Thorsett S. E., 1994, *Astrophysical Journal*, 422, 671
 Aschwanden M. J., et al., 2018, *Space Science Reviews*, 214, 1
 Baddeley A., Rubak E., Turner R., 2015, *Spatial point patterns: Methodology and applications with R*. Chapman and Hall/CRC, London
 Bartlett M. S., 1964, *Biometrics*, 20, 891
 Cheng K. S., Pines D., Alpar M. A., Shaham J., 1988, *Astrophysical Journal*, 330, 835
 Çinlar E., 1975, *Introduction to stochastic processes*. Englewood Cliffs, N.J. : Prentice-Hall
 Cordes J. M., Helfand D. J., 1980, *The Astrophysical Journal*, 239, 640
 Cox D. R., Lewis P. A. W., 1966, *The Statistical Analysis of Series*

of Events. Monographs on Statistics and Applied Probability, Chapman and Hall
 Espinoza C. M., Lyne A. G., Stappers B. W., Kramer M., 2011, *Monthly Notices of the Royal Astronomical Society*, 414, 1679
 Espinoza C. M., Antonopoulou D., Stappers B. W., Watts A., Lyne A. G., 2014, *Monthly Notices of the Royal Astronomical Society*, 440, 2755
 Ferdman R. D., Archibald R. F., Gourgouliatos K. N., Kaspi V. M., 2017, *The Astrophysical Journal*, 852, 123
 Fuentes J. R., Espinoza C. M., Reisenegger A., Shaw B., Stappers B. W., Lyne A. G., 2017, *A&A*, 608, A131
 Fulgenzi W., Melatos A., Hughes B. D., 2017, *Monthly Notices of the Royal Astronomical Society*, 470, 4307
 Gelfand A., Diggle P., Fuentes M., Guttorp P., eds, 2010, *Handbook of Spatial Statistics*. CRC Press, doi:10.1201/EBK1439803561-c0
 Gelman A., Carlin J. B., Stern H. S., Dunson D., Vehtari A., Rubin D. B., 2013, *Bayesian data analysis*, 3rd edn. Chapman and Hall/CRC, New York
 Groth E. J., 1975, *Astrophysical Journal Supplement Series*, 29, 431
 Gullahorn G. E., Isaacman R., Rankin J. M., Payne R. R., 1977, *Astronomical Journal*, 82, 309
 Haskell B., Melatos A., 2015, *International Journal of Modern Physics D*, 24, 1530008
 Hobbs G., Lyne A. G., Kramer M., 2010, *Monthly Notices of the Royal Astronomical Society*, 402, 1027
 Howitt G., Melatos A., Delaigle A., Hall P., in press 2018, *Astrophysical Journal*
 Jafari-Mamaghani M., 2010, *Frontiers in Neuroinformatics*
 Jeffreys H., 1998, *The Theory of Probability*, 3rd edn. OUP Oxford
 Jensen H. J., 1998, *Self-organized criticality. Emergent complex behavior in physical and biological systems*. Cambridge university press
 Kagan Y. Y., 2011, *Geophysical Journal International*, 186, 1347
 Kagan Y. Y., Jackson D. D., 1991, *Geophysical Journal International*, 104, 117
 Kass R. E., Raftery A. E., 1995, *Journal of the American Statistical Association*, 90, 773
 Keith M. J., Shannon R. M., Johnston S., 2013, *Monthly Notices of the Royal Astronomical Society*, 432, 3080
 Kenkel N. C., 1988, *Ecology*, 69, 1017
 Kingman J. F. C., 1993, *Poisson processes*. Oxford studies in probability: 3, Oxford: Clarendon Press; New York: Oxford University Press, 1993.
 Lagache T., Lang G., Sauvonnnet N., Olivo-Marin J.-C., 2013, *PLoS ONE*, 8, e80914
 Lang G., Marcon E., 2010, *ESAIM: Probability and Statistics*, 17, 767
 Larson M. B., Link B., 2002, *Monthly Notices of the Royal Astronomical Society*, 333, 613
 Lilliefors H. W., 1969, *Journal of the American Statistical Association*, 64, 387
 Loh J. M., 2008, *The Astrophysical Journal*, 674, 636
 Lohsen E. H. G., 1981, *Astronomy and Astrophysics Supplement Series*, 44, 1
 Lyne A. G., Pritchard R. S., Smith F. G., 1988, *Monthly Notices of the Royal Astronomical Society*, 233, 667
 Lyne A. G., Pritchard R. S., Graham Smith F., 1993, *Monthly Notices of the Royal Astronomical Society*, 265, 1003
 Lyne A. G., Jordan C. A., Graham-Smith F., Espinoza C. M., Stappers B. W., Weltevredre P., 2015, *Monthly Notices of the Royal Astronomical Society*, 446, 857
 McElreath R., 2016, *Statistical Rethinking: A Bayesian Course with Examples in R and Stan*. Chapman & Hall/CRC Texts in Statistical Science, CRC Press
 Melatos A., Peralta C., Wytke J. S. B., 2008, *The Astrophysical*

- [Journal](#), 672, 1103
- Melatos A., Howitt G. A. W., Fulgenzi W., 2018, [Astrophysical Journal](#), 863, 196
- Middleditch J., Marshall F. E., Wang Q. D., Gotthelf E. V., Zhang W., 2006, [The Astrophysical Journal](#), 652, 1531
- Negi P. S., 2007, [Astrophysics and Space Science](#), 332, 145
- Omori F., 1894, Journal of the College of Science, Imperial University of Tokyo, 7, 111
- Peterson C. J., Squiers E. R., 1995, [Journal of Ecology](#), 83, 847
- Piessens R., de Doncker-Kapenga E., Ueberhuber C. W., 1983, Quadpack. A subroutine package for automatic integration. Springer, Berlin
- Ripley B. D., 1977, [Journal of the Royal Statistical Society. Series B \(Methodological\)](#), 39, 172
- Ripley B. D., 1988, Statistical Inference for Spatial Processes. Cambridge University Press, Cambridge, doi:10.1017/CBO9780511624131
- Shaw B., et al., 2018, [Monthly Notices of the Royal Astronomical Society](#)
- Taylor J. H., Manchester R. N., Lyne A. G., 1993, [VizieR Online Data Catalog](#), 7156
- Turcotte D. L., 1999, [Reports on Progress in Physics](#), 62, 1377
- Utsu T., Ogata Y., S R., Matsu'ura 1995, [Journal of Physics of the Earth](#), 43, 1
- Vega Orozco C., Tonini M., Conedera M., Kanveski M., 2012, [GeoInformatica](#), 16, 653
- Warszawski L., Melatos A., 2011, [Monthly Notices of the Royal Astronomical Society](#), 415, 1611
- Warszawski L., Melatos A., 2013, [Monthly Notices of the Royal Astronomical Society](#), 428, 1911
- Warszawski L., Melatos A., Berloff N. G., 2012, [Physical Review B - Condensed Matter and Materials Physics](#), 85
- White A. C., Barengi C. F., Proukakis N. P., 2012, [Physical Review A - Atomic, Molecular, and Optical Physics](#), 86
- Yu M., et al., 2013, [Monthly Notices of the Royal Astronomical Society](#), 429, 688
- Yunta M. L., Lagache T., Santi-Rocca J., Bastin P., Olivo-Marin J.-C., 2014, in International Symposium on Biomedical Imaging. , doi:10.1109/ISBI.2014.6867928

This paper has been typeset from a \LaTeX file prepared by the author.